JOURNAL OF CATALYSIS 148, 205–212 (1994)

# Hydrotalcites as Base Catalysts: Influence of the Chemical Composition and Synthesis Conditions on the Dehydrogenation of Isopropanol

A. Corma,[1] V. Fornés, and F. Rey

*Instituto de Tecnología Química, UPV-CSIC, Universidad Politécnica de Valencia, Camino de Vera s/n, 46071 Valencia, Spain*

Received November 23, 1993; revised January 31, 1994

**Hydrotalcites with different Al/Al + Mg ratios, and prepared at different pH and different aging temperatures of the gel were used as precursors of Mg–Al mixed oxides, and their textural and physicochemical properties were determined. A complete reaction network for the isopropanol decomposition on these catalysts has been established, and it is shown that the concentration of acetone in the products cannot always be used for a direct estimation of the rate of dehydrogenation. The Al/Al + Mg ratio for which the maximum in activity is obtained depends on the base strength needed for each particular reaction. For dehydrogenation of isopropanol, this is found at Al/Al + Mg ≈ 0.25.** © 1994 Academic Press, Inc.

## INTRODUCTION

There is strong incentive to develop solid base catalysts which could efficiently carry out reactions such as alkylations, condensations, isomerizations, etc. under environmental friendly conditions. In this way, alkaline earth and mixed oxides (1), zeolites (2), fibrous materials such as chrysotile (4), crocidolite (5) or sepiolites (3), carbons and modified carbons (6), and basic resins (7) have been studied. Among those, the oxides produced by calcination of hydrotalcites (8) are the ones which, at present, look most promising as strong base solid catalysts. Indeed, these materials, when heated at temperatures higher than 400°C, produce partially dehydroxylated mixed oxides (9, 10) with basic strengths in the order of $H_0 = 17$ (11). The formation of $Mg_6Al_2O_9$ solid base materials from Mg–Al hydrotalcite by controlled heating has been studied (12, 13), and it appears that the active surface sites include the hydroxide ions as well as a range of $O^{2-}$–$M^{n+}$ acid–base pairs (12).

The number and strength of basic sites depend on chemical composition and activation conditions (12). The sites can catalyze aldol (14, 15) and Knoevenagel (16) condensations, H–D exchange (15), olefin isomerization (17), aromatization (18), and polymerization of propylene oxide (19, 20), and β-propiolactone (21).

The calcined hydrotalcite materials have a very disordered structure (22, 23), and it appears to us that the control of chemical composition and textural properties of the final materials through the control of the synthesis of the precursor could be of interest in designing hydrotalcite-derived basic catalysts.

In this work we have synthesized hydrotalcites with different chemical compositions and different crystallite sizes. The catalytic activity of the basic oxides produced upon calcination has been studied in the dehydrogenation and dehydration of 2-propanol to ketone and propylene, respectively. In this way, the correlation between the preparation conditions and base–acid properties of the calcined materials could be established.

## EXPERIMENTAL

### *Catalysts*

Hydrotalcites were prepared from the gels produced by mixing two solutions (A, containing $Mg(NO_3)_2$ and $Al(NO_3)_3$ 1.5 *M* in Al + Mg, with Al/(Al + Mg) atomic ratios equal to 0.20, 0.25, and 0.33 (Table 1) and B, prepared by dissolving $Na_2CO_3$ and NaOH to achieve a $Na_2CO_3$ concentration equal to 1 *M*) at 60 ml $h^{-1}$ addition rate for 4 h with vigorous stirring. The concentration of NaOH was adjusted to obtain pH = 13 or pH = 10 (Table 1). The gels were aged at different temperatures for 18 h (Table 1), and then filtered and washed until pH = 7. After drying the solids at 80°C for 12 h, the hydrotalcites were calcined at 450°C for 18 h in air in order to obtain Mg–Al mixed oxides. As a reference a MgO sample was prepared following the procedure previously reported by Matsuda *et al.* (24).

[1] To whom correspondence should be addressed.



0021-9517/94 $6.00
Copyright © 1994 by Academic Press, Inc.
All rights of reproduction in any form reserved.

TABLE 1

Synthesis Conditions of Hydrotalcite

| Sample | Gel composition | pH | Aging temp. (K) | $(Al/Al + Mg)_{gel}$ ratio |
|---|---|---|---|---|
| HT1 | $2Mg(NO_3)_2 : 1Al(NO_3)_3 : 2Na_2CO_3 : 5NaOH$ | 10 | 473 | 0.33 |
| HT2 | $2Mg(NO_3)_2 : 1Al(NO_3)_3 : 2Na_2CO_3 : 7NaOH$ | 13 | 473 | 0.33 |
| HT3 | $2.25Mg(NO_3)_2 : 0.75Al(NO_3)_3 : 2Na_2CO_3 : 6.75NaOH$ | 13 | 473 | 0.25 |
| HT4 | $2.4Mg(NO_3)_2 : 0.6Al(NO_3)_3 : 2Na_2CO_3 : 6.6NaOH$ | 13 | 473 | 0.20 |
| HT5 | $2.25Mg(NO_3)_2 : 0.75Al(NO_3)_3 : 2Na_2CO_3 : 6.75NaOH$ | 13 | 333 | 0.25 |

*Apparatus and Methods*

X-ray powder diffraction patterns were obtained on a Philips 1010 diffractometer equipped with a graphite monochromator using Cu$K\alpha$ radiation.

IR spectra were recorded on a FTIR Nicolet 710 spectrometer employing the KBr dilution technique.

$^{27}$Al-MAS NMR spectra were obtained on a Varian Unity VRX-400 WB spectrometer at ambient temperature and at 104.2 MHz using a Varian MAS probe with zirconia rotors (7 mm diameter). The length of the rf pulses was 0.6 $\mu$s (flip angle = $\pi/20$) and the spinning frequency 7–9 KHz. A total amount of 1500 fids were accumulated and a time interval of 0.5 s between successive fids was selected to avoid saturation effects. All measurements were carried out at room temperature with $Al(H_2O)_6$ as standard reference. The mean error in the measured isotropic chemical shift was 0.5 ppm.

Surface area and pore distribution were determined by $N_2$ adsorption–desorption in a Micromeritics ASAP 2000 instrument using the BET equation for surface area and the BJH method for pore distribution calculations. Prior to the measurements, samples were pretreated at 673 K under vacuum overnight.

*Reaction Procedure*

Isopropanol was introduced into a vaporizer heated at 350°C, by means of a positive displacement pump. There, it was mixed with $N_2$ to obtain a molar isopropanol/$N_2$ ratio equal to 1. This mixture was introduced into a glass tubular reactor heated at 350°C connected on-line with a gas chromatograph. 0.40 g of catalyst was used in all experiments and the flow of the feed was adjusted to obtain a F/W ratio equal to 0.39 $mole_{isopropanol}\ g_{cat}^{-1}\ h^{-1}$. The reaction products were separated in a 15-m trifluoropropylmethylsilicone semicapillary column and identified by mass spectrometry.

## RESULTS AND DISCUSSION

*Catalyst Characterization*

The hydrotalcite precursors as well as the final catalysts were characterized by XRD, IR, and $^{27}$Al MAS-NMR spectroscopies. In Table 1 the chemical compositions, temperatures of aging, and pH of the synthesis gels are summarized. Bulk elemental analysis, surface area, and average crystal sizes of calcined hydrotalcites (CHT) are included in Table 2.

The XRD diagrams, shown in Fig. 1, suggest that pure hydrotalcite was formed in all cases except for HT1 sample (pH = 10 and an Al/(Al + Mg) ratio equal to 0.33). Under these conditions a mixture of Manasseite and $Mg_2Al(OH)_6(OH)$ was obtained. Both compounds are closely related with the hydrotalcite structure since Manasseite is built by brucite-like layers in a similar way to hydrotalcite but with a different stacking order (25). On the other hand, the difference between the $Mg_2Al(OH)_6(OH)$ compound and hydrotalcite is that the exchangeable anions situated in the interlayer space are hydroxides instead of carbonate (26).

TABLE 2

Chemical Composition and Textural and Acidic Properties at Catalysts

| Sample | $(Al/Al + Mg)_{solid}$ ratio | Surface area ($m^2\ g^{-1}$) | Crystal size (nm) | Morphology | $NH_3$ adsorbed (moles $m^{-2} \times 10^7$) |
|---|---|---|---|---|---|
| HT1 | 0.33 | 164 | 500 | Hexagonal plates | 2.981 |
| HT2 | 0.30 | 175 | 500 | Hexagonal plates | 3.023 |
| HT3 | 0.25 | 177 | 200–500 | Hexagonal plates | 2.714 |
| HT4 | 0.20 | 189 | Not measured | Not measured | Not measured |
| HT5 | 0.25 | 240 | <50 | Spherical particles | 3.199 |
| MgO | 0 | 200 | <10 | Not measured | 0 |

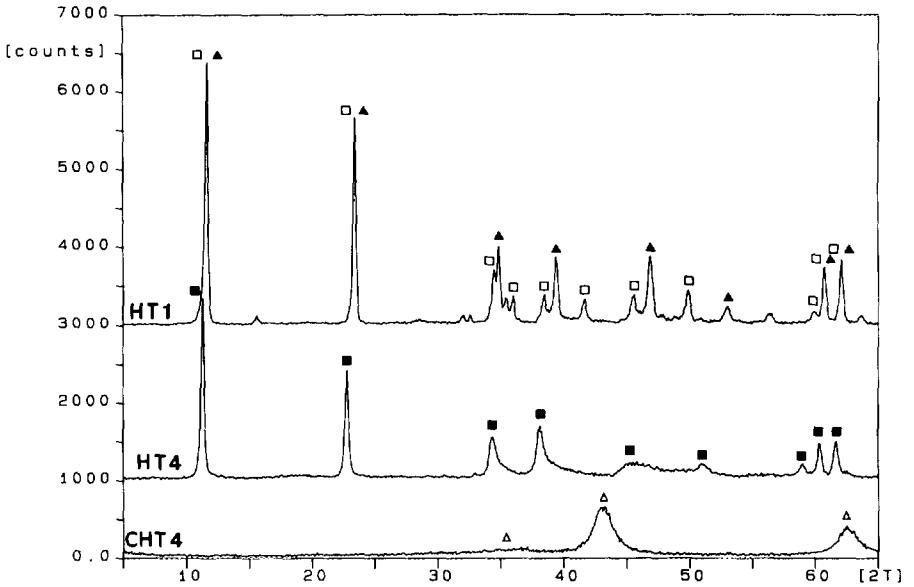


FIG. 1. XRD patterns of HT1, HT4, and calcined HT4 (CHT4). Hydrotalcite (■); $Mg_2Al(OH)_6(OH)$ (▲); manasseite (□); MgO (△).

In Fig. 2, the variation of the lattice parameter *a* of the hydrotalcites versus their Al content has been presented. It can be seen there that a linear correlation between both variables exists, as a consequence of the smaller ionic radius of $Al^{3+}$ as compared with $Mg^{2+}$ cations (27, 28). This is strong evidence that the $Mg^{2+}$ is isomorphically substituted by $Al^{3+}$ in the hydrotalcite framework.

The $^{27}Al$ MAS–NMR spectra shown in Fig. 3 (HT3) is consistent with the above conclusion. Indeed, only a signal centered at 9 ppm is observed in the original hydrotalcite. This band has been assigned to Al octahedrally coordinated to OH groups in the hydrotalcite (29).

When the hydrotalcite samples were calcined at 450°C for 18 h to obtain the basic Mg–Al mixed oxides, the XRD spectra of the resultant materials could be assigned to a poorly crystallized MgO (Fig. 1c), but with a lattice constant slightly smaller than that of pure MgO (Fig. 4). This result indicates that $Al^{3+}$ are also substituting isomorphically $Mg^{2+}$ cations in the mixed oxides (27). The positive charge generated by this isomorphous substitution could be compensated by the formation of two types of defects:

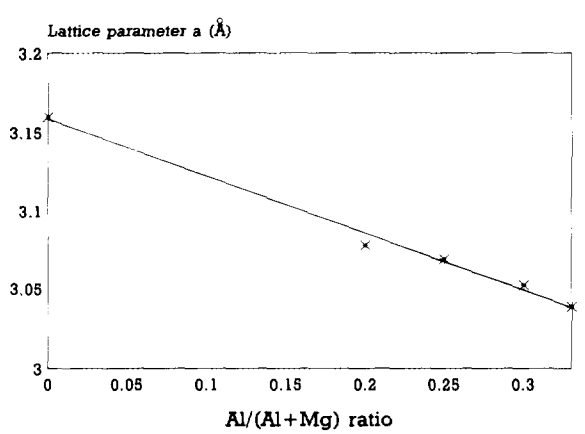


FIG. 2. Lattice parameter *a* as a function of the Al/(Al + Mg) ratio of hydrotalcites.

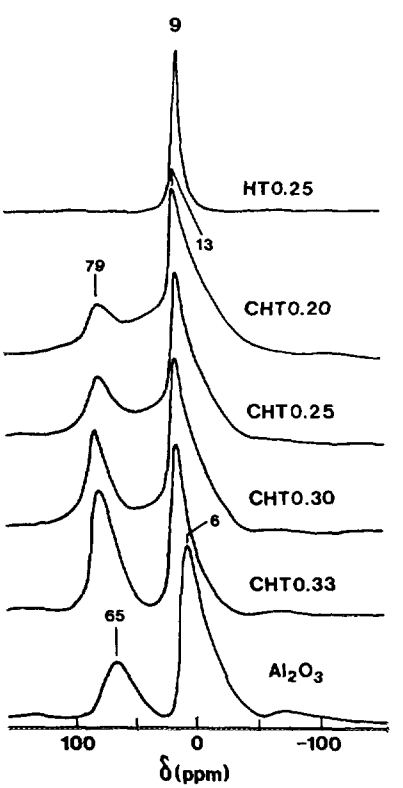


FIG. 3. $^{27}Al$ MAS–NMR spectra of hydrotalcite (HT), calcined hydrotalcite (CHT), and pure γ-alumina.

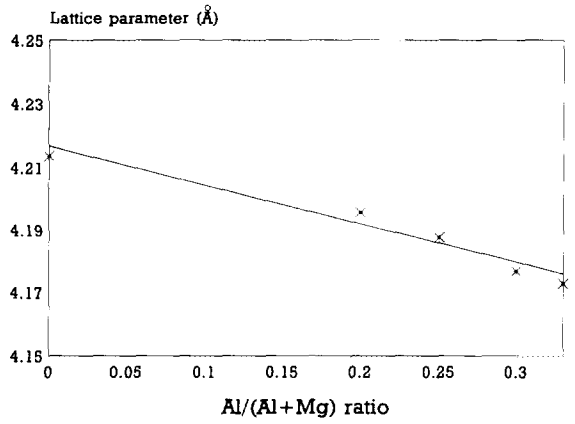


FIG. 4. Lattice parameter $a$ as a function of the Al/(Al + Mg) ratio of calcined hydrotalcites (CHT).

cationic vacancies and/or inclusion of intersticial oxygens in the structure. The formation of the first type of defects is the mechanism generally accepted in order to compensate the cationic excess in these mixed oxides (22, 29). However, this model does not explain the appearance of a new line at 69 ppm in the $^{27}Al$ MAS–NMR spectra (Fig. 3) and a new band at 850 $cm^{-1}$ in the IR spectra (not shown), both assigned to Al tetrahedrally coordinated (30, 31). It has to be pointed out that the amount of tetrahedral aluminum increases with increasing the Al/(Al + Mg) ratio in the HTC. The presence of tetrahedral aluminum has been attributed to formation of $\gamma$-$Al_2O_3$ (12), but the $Al_{Td}/Al_{OH}$ ratios and chemical shifts of Al signals observed do not correspond with those in $\gamma$-$Al_2O_3$ (see Fig. 3). Moreover, the capacity of the mixed oxides to easily regenerate the original hydrotalcite when exposed to water indicates that the formation of extensive amounts of $\gamma$-$Al_2O_3$ is very improbable (13). Therefore, it can be admitted that at least a part of the tetrahedral aluminum is located at tetrahedral positions in MgO lattice. This structure could give rise to the formation of clusters of Mg–Al inverse spinel type, as has been proposed in the literature (28, 32). The high instability of this structure could explain the metaestable character of the Mg–Al mixed oxide formed by calcination of hydrotalcites. The $Al^{3+}$ located at the tetrahedral or octahedral sites produces the defect of $Mg^{2+}$ or $Al^{3+}$ in the framework in order to compensate the positive charge generated. The $O^{2-}$ ions adjacent to the $Mg^{2+}/Al^{3+}$ defects become coordinatively unsaturated and could provide strong basic sites.

The textural properties of calcined hydrotalcites are shown in Fig. 5. It can be seen there that the surface area strongly increases when the hydrotalcite is synthesized at lower temperature (Fig. 5a). This increase of surface area is accompanied in the pore distribution by an increase of mesoporosity (50–150 Å) (Fig. 5b). On the other hand no dependence was found between the textural properties and the Al/(Al + Mg) ratio in the calcined hydrotalcites.

*Catalytic Results*

*Reaction network.* Under the experimental conditions used here several reaction products were obtained on the CHT catalysts:

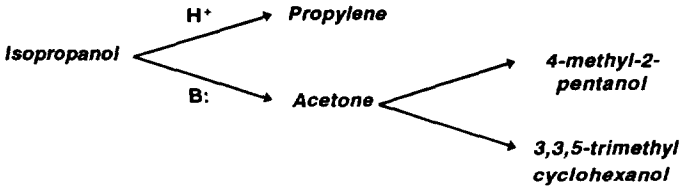


When the yields are plotted versus the total conversion (Fig. 6), it can be seen that the products from dehy-

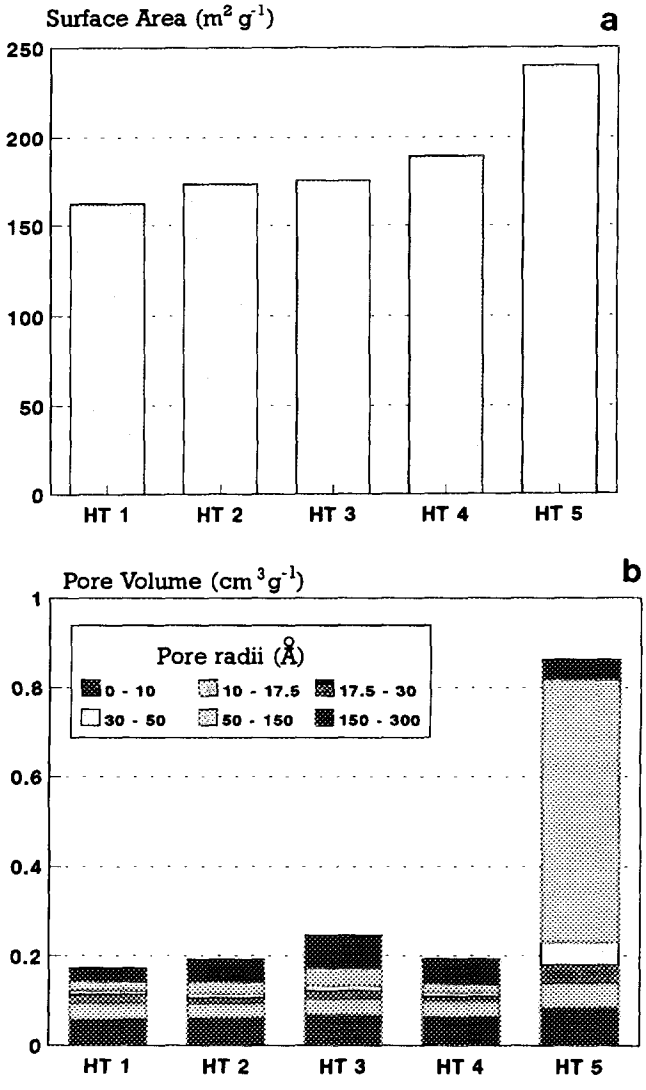


FIG. 5. Surface area (a) and pore size distribution (b) for the different calcined hydrotalcites.

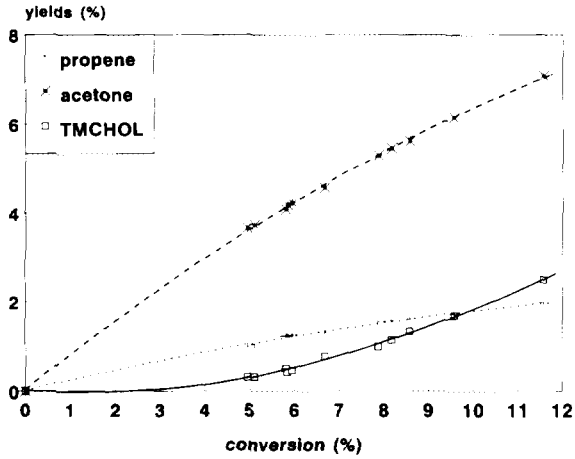


FIG. 6. Selectivity of CHT versus total conversion.

drogenation and dehydration reactions, i.e., acetone and propylene, respectively, behave as primary and unstable products, whereas 3,3,5-trimethylcyclohexanol (TMCHOL) appears as a secondary and stable product. The 4-methyl-2-pentanol (4M2POL) is obtained in very low concentrations and it becomes difficult to assert its kinetic behavior.

The fact that acetone appears as an unstable product can be explained by considering that it reacts with another molecule of acetone through an aldol-type condensation (14,33) to form 4-methyl-3-penten-2-one (mesityl oxide).

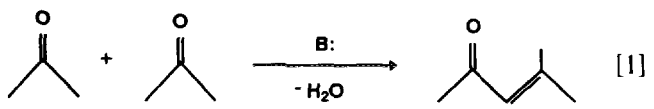


*mesytil oxide* [1]

This would react rapidly with isopropanol in a series of consecutive reactions to give TMCHOL as the final product. The global process can occur through reactions [2]–[4], also catalyzed by bases, and which involve a Meerving–Pondorf reaction of mesityl oxide with acetone (33, 34), an aldol condensation to form isophorone (14), and the hydrogen transfer from isopropanol to isophorone (34), respectively.

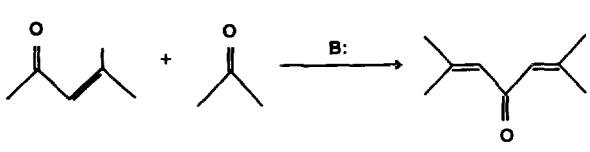


*phorone* [2]

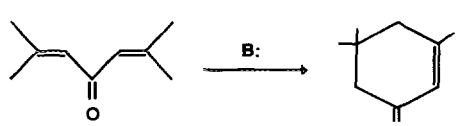


[3]

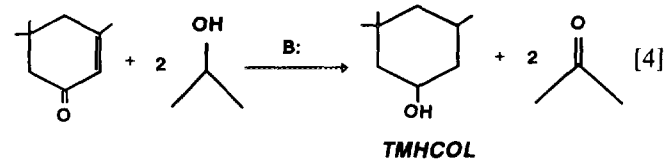


*TMHCOL* [4]

Finally, 4M2POL is obtained from the reaction of mesytil oxide with isopropanol, reaction [5].


*4M2POL* [5]

The unstable character of propylene could be attributed to the formation of coke on the catalyst surface by polymerization reactions on the acid sites present in the catalyst (35).

The possibility for the formation of 4M2POL and TMCHOL through the reactions presented above was proved, since high yields of these two products were obtained when reacting acetone with isopropanol under the same experimental conditions. Finally, reaction [4] was also proved to occur under those experimental conditions, since when isophorone and isopropanol were fed into the reactor, 100% of conversion of isophorone to TMCHOL was achieved.

It has to be pointed out that acetone is formed in the hydrogen transfer reaction from isopropanol to mesytil oxide and isophorone to TMCHOL (34). In other words, the reaction scheme found for the reaction of acetone on hydrotalcites clearly shows that acetone is formed and consumed in reactions other than the dehydrogenation of isopropanol. This indicates that the concentration of acetone cannot be taken as a measure of the dehydrogenation reaction. Thus, taking into account the acetone mass balance derived from the reaction network one can establish that the rate of dehydrogenation of isopropanol has to be calculated from the equation

Isopropanol dehydrogenation conversion

$$= [\text{acetone}] - [\text{TMCHOL}]. \quad [6]$$

When the decomposition of isopropanol was carried out over CHT catalysts, in addition to acetone, propylene was also observed. These results indicate that the calcined hydrotalcites have both acid and basic sites (35, 36). Moreover, calcined hydrotalcites have basic sites capable of catalyzing consecutive reactions of acetone such as aldolic condensation and hydrogen transfer. It has to be remarked that on the MgO prepared catalyst only acetone was detected as reaction product, and no further reaction of the primarily formed acetone was observed.

*Influence of the Al content and crystallite size of the hydrotalcite on catalytic activity and selectivity.* From the structural point of view the number of defects, and therefore the number of strong basic sites, in the lattice of MgO should be expected to increase when increasing the amount of Al introduced. On the other hand, and since Al is more electronegative than Mg, an increase in Al should increase the average electronegativity of the solid and thus, a decrease in the average electronic density of the unsaturated framework oxygens could be expected, with the corresponding effect on their basic strength.

If this is true, then reactions demanding different base strength should give a maximum in activity at different Al/Al + Mg compositions. Thus, the more demanding a reaction is, from the point of view of the basic strength needed, the lower the Al/Al + Mg ratio at which the maximum in activity is observed should be.

The results in Fig. 7 show that, when the activity at different times on stream for the CHT with different Al/Al + Mg ratios was calculated taking into account Eq. [6], the catalysts become deactivated, probably due to the formation of polymers from acetone and/or propylene. However, it should be noted that the selectivity to the different products also changes with time on stream.

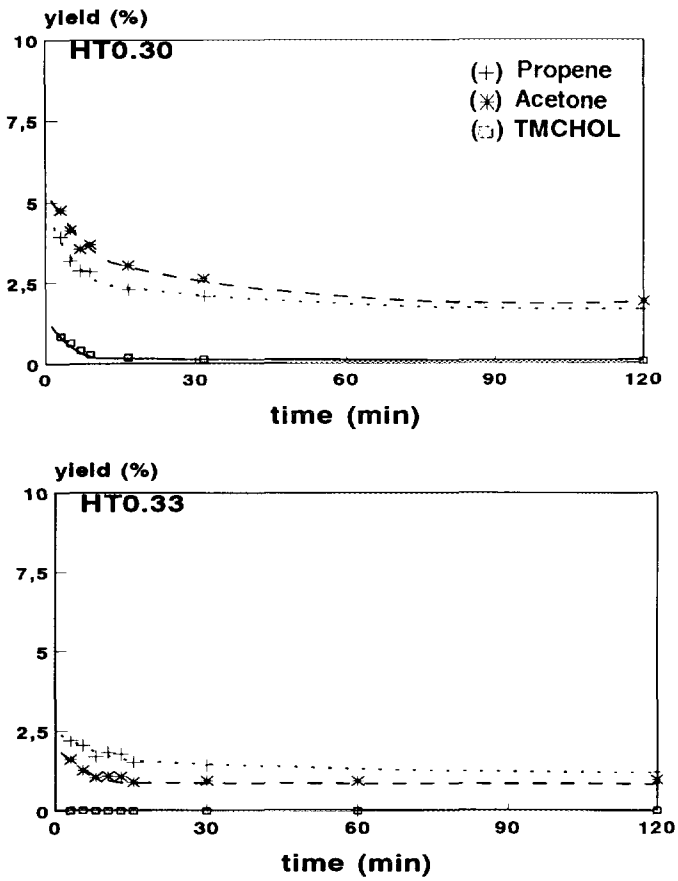


FIG. 7. Activity versus time on stream for samples CHT4 and MgO.

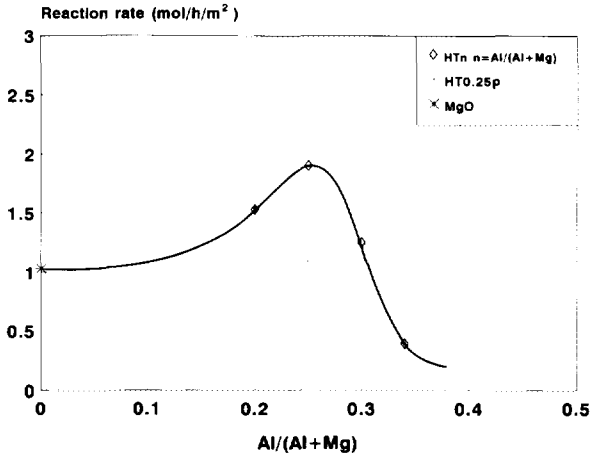


FIG. 8. Initial reactivity as a function of the Al/(Al + Mg) ratio.

Then, it becomes clear that different conclusions could be obtained depending on at what time on stream the catalytic properties of the catalysts are measured. To avoid this problem, the catalytic activity and selectivity of the different catalysts have been compared here at zero time on stream, by extrapolating the curves from Fig. 7.

In this way, Fig. 8 shows that a maximum in the rate of dehydrogenation of isopropanol to acetone exists for an Al/Al + Mg ratio of ~0.25. In the case of TMCHOL, the maximum is shifted to a lower Al/Al + Mg ratio (Fig. 9). On the basis of the model described above, these results would indicate that reactions conducting to the formation of TMCHOL need stronger basic sites than the dehydrogenation of isopropanol to acetone.

The propylene formation on the CHT samples can be related to the presence of acid sites associated to $Al^{3+}$, which is substituted by $Mg^{2+}$ in a MgO lattice. This substitution may produce local excesses of positive charge in the lattice of the oxide which can act as acid sites (35,

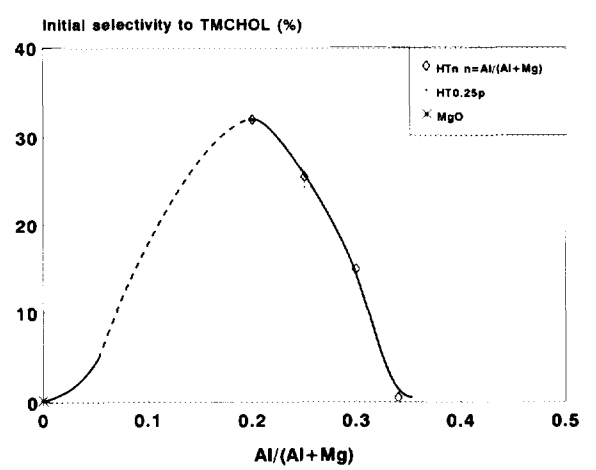


FIG. 9. Initial selectivity to TMCHOL as a function of the Al/(Al + Mg) ratio.

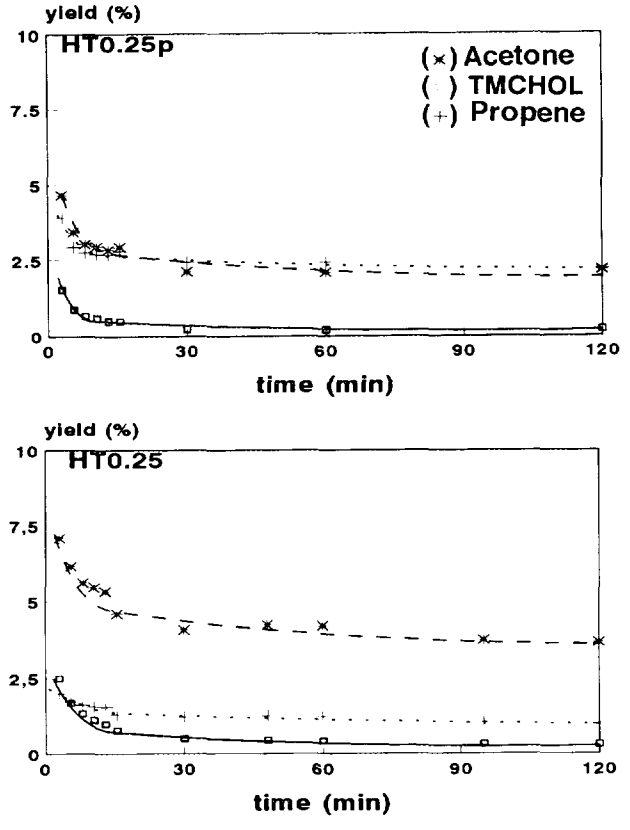


FIG. 10. Influence of crystal size of HT on activity and selectivity of final catalysts (CHT).

36). Indeed, the $NH_3$ TPD results from Table 2 show that calcined hydrotalcites adsorb ammonia, while MgO does not.

The effect of the crystal size of the starting hydrotalcite on the final activity and selectivity of two CHT samples with the same Al/Al + Mg ratio (Tables 1 and 2) is presented in Fig. 10. There, it can be observed that the sample with smaller crystal size (HT5) is less active than that with larger crystals (HT3); however, a similar acetone/TMCHOL ratio is observed on both samples. This could be explained assuming that the incorporation of Al in the lattice of MgO is smaller in the HT5 (HT0.25p) sample, probably due to the fact that a larger segregation of alumina occurred during the calcination of the smaller crystallite sample.

## CONCLUSIONS

Hydrotalcites with different Al/Al + Mg ratios were used as starting materials to produce by calcination Mg–Al mixed oxides in which $Al^{3+}$ are substituting isomorphically $Mg^{2+}$ cations in the MgO framework. The surface area of the mixed oxides increases when decreasing the temperature of the synthesis of the precursor hydrotalcite.

During the reaction of isopropanol on calcined hydrotalcites, acetone, propylene, TMCHOL, and 4M2POL are also formed. Acetone is consumed and formed in consecutive reactions, and therefore its concentration in the products cannot be used as a direct measurement of the rate of dehydrogenation of isopropanol.

A maximum in dehydrogenation activity has been found for samples with an Al/Al + Mg ratio of ~0.25. The more demanding in basicity the reaction is, the lower the Al/Al + Mg ratio at which the maximum in activity is found.

## ACKNOWLEDGMENT

Financial support by the Dirección General de Investigación Científica y Técnica of Spain (Project MAT 91-1097-CO2-01) is gratefully acknowledged.

## REFERENCES

1. Tanabe, K., *in* "Catalysis by Acids and Bases" (B. Imelik *et al.*, Eds.), p. 1. Elsevier, Amsterdam/New York, 1985.
2. Corma, A., Fornés, V., Martín-Aranda, R. M., García, H., and Primo, J., *Appl. Catal.* **59,** 237 (1990).
3. Corma, A., and Martín-Aranda, R. M., *J. Catal.* **130,** 130 (1991).
4. Bonneau, L., and Pezerat, H., *J. Phys. Chem.* **80,** 275 (1983).
5. Graceffa, P., and Weitzman, S. A., *Arch. Biochem. Biophys.* **257,** 481 (1987).
6. Csuk, R., Glanzer, B. I. and Furstner, A., *Adv. Organomet. Chem.* **28,** 85 (1988).
7. Sherrintong, D. C., *in* "Polymer-Supported Reactions in Organic Synthesis" (P. Hodge and D. C. Sherringtong, Eds.), Chap. 3. Wiley, New York, 1980.
8. Cavani, F., Trifiró, F., and Vaccari, A., *Catal. Today* **11,** 173 (1992).
9. Miyata, S., *Clays Clay Miner.* **28,** 50 (1980).
10. Rouxhet, P. G., and Taylor, H. F. W., *Chimia* **23,** 480 (1969).
11. Miyata, S., Kumura, T., Hattori, H., and Tanabe, K., *J. Chem. Soc. Jpn.* **92,** 514 (1971).
12. Reichle, T., Kang, S. Y., and Everhardt, D. S., *J. Catal.* **101,** 352 (1986).
13. Rey, F., Fornés, V., and Rojo, J. M., *J. Chem. Soc., Faraday Trans.* **88,** 2233 (1992).
14. Reichle, W. T., *J. Catal.* **94,** 547 (1985).
15. Reichle, W. T., US Patent 4,458,086 (1984).
16. Corma, A., Fornés, V., Martín-Aranda, R. M., and Rey, F., *J. Catal.* **134,** 58 (1992).
17. Scharper, H. S., Berg-Slot, J. J., and Stork, W. H. J., *Appl. Catal.* **54,** 79 (1989).
18. Davis, R. J., and Derouane, E. G., *J. Catal.* **132,** 269 (1991).
19. Laycock, D. E., Collacott, R. J., Skelton, D. A., and Tchir, M. T., *J. Catal.* **130,** 354 (1991).
20. Kohjiya, S., Sato, T., Nakayama, T., and Yamashita, S., *Makromol. Chem., Rapid. Coimmun.* **2,** 231 (1981).
21. Nakatsuka, T., Kawasaki, H., Yamashita, S., and Kohjiya, S., *Bull. Chem. Soc. Jpn.* **52,** 2449 (1979).
22. Sato, T., Wakahayashi, T., and Shimada, M., *Ind. Eng. Chem. Prod. Res. Dev.* **25,** 89 (1986).
23. Hernández, M. J., Ulibarri, M. A., Rendon, J. L., and Serna, C. J., *Thermochim. Acta* **81,** 311 (1984).
24. Matsuda, T., Ishimatsu, K., and Sugimoto, M., *React. Kinet. Catal. Lett.* **44,** 63 (1991).

25. Taylor, H. F. W., *Mineral. Mag.* **39,** 377 (1973).
26. Mascolo, G., and Marino, O., *Mineral. Mag.* **43,** 619 (1980).
27. Sato, T., Fujita, H., Endo, T., Shimada, M., and Tsunashima, A., *React. Solids* **5,** 219 (1988).
28. Derouane, E. G., Jullien-Lardot, V., Davis, R. J., Blom, N., and Höjlund-Nielsen, P. E., *Prep. X Inter. Congr. Catal., Budapest* **B,** 1031 (1993).
29. Carrol, J. C. G., Corish, J., Henderson, B., and Mackrodt, W. C., *J. Mater. Sci.* **23,** 2824 (1988).
30. Engelhard, G., and Michel, D., "High Resolution Solid State NMR of Silicates and Zeolites." Wiley, New York, 1987.
31. Farmer, V. C., *in* "The Infrared Spectra of Minerals," Monograph 4. Mineralogical Society, London 1974.
32. Asakura, K., and Iwasawa, Y., *Mater. Chem. Phys.* **18,** 499 (1988).
33. Tomczak, D. C., Thong, S. H., and Poeppelmeier, K. R., *Catal. Lett.* **12,** 139 (1992).
34. Kaspar, J., Trovarelli, A., Lenarda, M., and Graziani, M., *Tetrahedron Lett.* **30,** 2705 (1989).
35. McKenzie, A. L., Fishel, C. T., and Davis, R. J., *J. Catal.* **138,** 547 (1992).
36. Kelkar, C. P., Schutz, A., and Marcelin, G., *ACS Symp. Ser.* **368,** 324 (1988).